Climate Dynamics (1998) 14:385–407

F. D'Andrea · S. Tibaldi · M. Blackburn · G. Boer
M. Déqué · M. R. Dix · B. Dugas · L. Ferranti
T. Iwasaki · A. Kitoh · V.Pope · D. Randall
E. Roeckner · D. Straus · W. Stern
H. Van den Dool · D. Williamson

Northern Hemisphere atmospheric blocking as simulated by 15 atmospheric general circulation models in the period 1979–1988

Received: 16 July 1997/Accepted: 20 October 1997

Abstract As a part of the Atmospheric Model Intercomparison Project (AMIP), the behaviour of 15 general circulation models has been analysed in order to diagnose and compare the ability of the different models in simulating Northern Hemisphere midlatitude atmospheric blocking. In accordance with the established AMIP procedure, the 10-year model integrations were performed using prescribed, time-evolving monthly mean observed SSTs spanning the period January 1979–December 1988. Atmospheric observational data (ECMWF analyses) over the same period have been also used to verify the models results. The models involved in this comparison represent a wide spectrum of model complexity, with different horizontal and vertical resolution, numerical techniques and physical parametrizations, and exhibit large differences in blocking behaviour. Nevertheless, a few common features can be found, such as the general tendency to underestimate both blocking frequency and the average duration of blocks. The problem of the possible relationship between model blocking and model systematic errors has also been assessed, although without resorting to ad-hoc numerical experimentation it is impossible to relate with certainty particular model deficiencies in representing blocking to precise parts of the model formulation.

1 Introduction

The present work has been conducted as part of the diagnostic subproject 10 of the AMIP (Atmospheric Model Intercomparison Project). AMIP is an international project aimed at producing a coordinated GCM

F. D'Andrea[1] (✉) · S. Tibaldi[2]
Atmospheric Dynamics Group, Department of Physics, University of Bologna, Italy

M. Blackburn
Department of Meteorology, University of Reading, UK

G. Boer
Canadian Centre for Climate Research, Victoria, Canada

M. Deque
Centre National de Recherches Météorologiques, Toulouse, France

M. R. Dix
Commonwealth Scientific and Industrial Research Organization, Mordialloc, Australia

B. Dugas
Recherhe en Prévision Numérique, Dorval, Canada

L. Ferranti
European Centre for Medium-Range Weather Forecasts, Reading, UK

T. Iwasaki
Numerical Prediction Division, Japan Meteorological Agency, Tokyo, Japan

A. Kitoh
Meteorological Research Institute, Tsukuba, Japan

U. Pope
Hadley Centre for Climate Prediction and Research, UK Meteorological Office, Bracknell, UK

D. Randall
Department of Atmospheric Science, Colorado State University, USA

E. Roeckner
Max-Plank-Institut für Meteorologie, Hamburg, Germany

D. Strauss
Center for Ocean-Land-Atmosphere Studies, Calverton, MD, USA

W. Stern
Geophysical Fluid Dynamics Laboratory/NOAA, Princeton University, USA

H. Van den Dool
National Meteorological Center, Washington DC, USA

D. Williamson
National Center for Atmospheric Research, Boulder , CO, USA

Present addresses:
[1]Laboratoire de Meteorologie Dynamique du CNRS, Paris, France
[2]Regional Meteorological Service of the Environmental Agency of Emilia-Romagna, Bologna, Italy

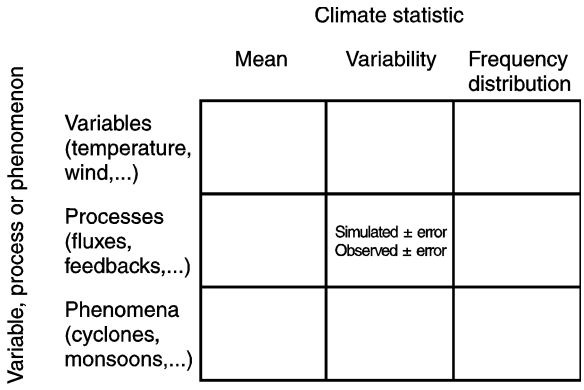

Fig. 1 The model diagnostics matrix, taken from Gates (1991)

diagnostic comparison. A description of the scope of the AMIP program, and a discussion about model validation as a problem of crucial importance in modern climate studies can be found in Gates (1992). In that work, a two-dimensional matrix approach to model diagnostics is proposed (Fig. 1). One axis represents the nature of the object of the diagnosis: prognostic variables, dynamical and physical processes or specific phenomena. The other axis represents the statistical detail with which the diagnosis is carried out, considering only mean values, variances (or some higher order statistical moments) or complete frequency distributions. A complete model diagnosis would take into account all the elements of the matrix and their possible interactions and relationships.

A challenging element in model validation is the diagnosis of specific phenomena. Such "phenomenon diagnostics" are challenging because of a general lack of standard methods, which often stimulates the development of new ideas. These may include the choice of the particular phenomenon to be diagnosed, the possible development of appropriate objective indices or the revisitation of more classical synoptic analysis techniques, as well as the study of new ways of visualisation. Phenomenon diagnostics can be a good tool to probe, and possibly improve, models in areas of their behaviour which often turn out to be deficient. Hitherto hidden problems (or unexpected levels of skill) are often brought to light in this way. Moreover, the diagnosis of small- or medium-scale phenomena is complementary to the more usual methods of testing GCM behaviour almost exclusively on time-mean planetary scales. Small- or medium-scale phenomena are, furthermore, often the end product of many scale interaction processes, sometimes also poorly diagnosed.

Many diagnostic studies are being conducted within the framework of the AMIP. Some examples in the literature regard interannual tropical rainfall (Sperber and Palmer 1995), tropical diabatic heating (Boyle 1995a), kinetic energy (Boyle 1995b), and a comprehensive study of intraseasonal oscillations by J. Slingo et al. (1995).

The present study is an example of phenomenon diagnostics, the phenomenon in this case being Northern Hemisphere atmospheric blocking. Blocking, in other words, will be the "peephole" through which all the models of the AMIP dataset will be observed. As will be seen, from this specific (and limited) viewpoint, it will be possible in some cases to make some inferences on the overall behaviour of the models, as well as on the behaviour of the real atmosphere. The scope of this work is, nonetheless, more concentrated on model intercomparison than on studying the dynamics or climatology of the observed blocking.

In Sect. 2, a description of the diagnostic method is given, as well as a list of the models analysed. Section 3 is devoted to a brief review of recent work on blocking, including both the modelling and the observational aspects. Section 4 reports on the main body of the diagnostic effort by comparing different statistical and synoptic aspects of blocking as simulated by the models. In Sect. 5, the relationship between the ability of models in reproducing blocking and their systematic errors is assessed. Section 6 contains some concluding remarks.

2 Datasets and methods

Systematic atmospheric blocking diagnostics, on both observed and model data, requires the definition of an objective blocking index through which model behaviour can be assessed. The index developed by Tibaldi and Molteni (1990, hereafter TM) was used for this purpose, albeit with a minor modification which will be described. This index requires daily fields of 500 hPa geopotential height (GPH). Model data were provided either by PCMDI (Program for Climate Models Diagnosis and Intercomparison) at Lawrence Livermore National Laboratory, which is the AMIP coordinating institute, or directly by the modelling groups. A list of all models considered is shown in Table 1, which also lists the model acronyms that will be used throughout. The letter in the first column of Table 1 will also be used throughout the figures to reference a model.

The integrations were carried out by the different modelling groups using the standardised conditions prescribed by AMIP, i.e. the models were integrated for 10 y from 1979 to 1988 and used the same set of observed monthly mean sea surface temperatures (SSTs) and sea ice, plus agreed values of the solar constant and of the current level CO_2 concentration (Gates 1992).

ECMWF operationally analysed 500 hPa geopotential height data for the same AMIP period 1979–1988 have been used to diagnose observed blocking for comparison with the modelled data. In some cases a longer ('climatological') dataset of observed data is used, spanning the period December 1949 - February 1994. This dataset was obtained merging NMC (1949–1979) and ECMWF (1980–1994) analyses.

More details about the participating models than those reported in Table 1 can be found in PCMDI report 18 (Phillips 1994), except for NMC (Kalnay et al. 1996), METEOFR (Déqué et al. 1994) and JMA (JMA 1993), which provide output produced by different models (or different versions of the models) with respect to the original AMIP models described in the report. As an overall reference on the general performance of each model, the Appendix

Table 1 List of the participating models, horizontal and vertical resolution and relevant comments. The letter in the first column is used in figure captions while the acronyms are used throughout the text to reference the corresponding model. In the Appendix Figs. (A1, A2 and A3), 500 hPa wintertime climate and variabilities are shown for each model

	Model Institute (and acronym)	Horizontal and vertical Resolution	Comments
a	ECMWF operational analysis (Analysis)	$3.75^\circ \times 3.75^\circ$	Observed analysis used for comparison
b	Canadian Climate Centre (CCC)	T32, L10	—
c	Center for Ocean-Land-Atmosphere Studies (COLA)	R40, L18	—
d	Commonwealth Scientific and Industrial Research Organization (CSIRO)	R21, L9	—
e	Colorado State University (CSU)	$4^\circ \times 5^\circ$, L17	—
f	DERF model of Geophysical Fluid Dynamics Laboratory (DERF/GFDL)	T42, L18	—
g	Max-Plank-Institut für Meteorologie (ECHAM)	T42, L19	—
h	European Centre for Medium-Range Weather Forecasts (ECMWF)	T42, L19	—
i	Japan Meteorological Agency (JMA)	T106, L21	New, high resolution version of the AMIP model
l	Centre National de Recherches Météorologiques (METEOFR)	T42, L30	ARPEGE model, not in the AMIP documentation
m	Meteorological Research Institute (MRI)	$4^\circ \times 5^\circ$, L15	—
n	National Center for Atmospheric Research (NCAR)	T42, L18	—
o	National Meteorological Center (NMC)	T42, L18	8 y 1985–1992 run, not in the AMIP documentation
p	Recherche en Prévision Numérique (RPN)	T63, L23	Data truncated at T21 on output
q	UK Universities Global Atmospheric Modelling Programme (UGAMP)	T42, L19	—
r	Hadley Centre for Climate Prediction, UK Meteorological Office (UKMO)	$2.5^\circ \times 3.75^\circ$, L19	—

Figs A1, A2 and A3 show mean 500 Pa and high- and low-frequency variability maps calculated from each model output.

As anticipated, the occurrence of blocking in all model output has been objectively diagnosed by making use of the TM. With respect to the original definition, however, one minor but important modification (in condition 2.5 below) was introduced here. The reasons for this are related to an improved definition of Pacific blocking and are discussed in detail in Giannini (1994).

The objective blocking index used throughout this work is then the following:
the geopotential height meridional gradients *GHGS* and *GHGN* are computed for each longitude:

$$GHGS = \frac{Z(\phi_0) - Z(\phi_S)}{\phi_0 - \phi_S} \tag{1}$$

$$GHGS = \frac{Z(\phi_n) - Z(\phi_0)}{\phi_n - \phi_0} \tag{2}$$

where

$$\phi_n = 78.75^\circ N + \Delta$$
$$\phi_0 = 60^\circ N + \Delta \tag{3}$$
$$\phi_S = 41.25^\circ N + \Delta$$

with

$$\Delta = -3.75^\circ, 0^\circ, 3.75^\circ.$$

A given longitude is then locally defined as blocked on a specific day if the following conditions are satisfied (for at least one of the three values of Δ):

$$\text{GHGS} > 0, \tag{4}$$

$$\text{GHGN} < -5 \text{ m/deg lat}, \tag{5}$$

Using a similar method to that in TM, the two main sectors of the Northern Hemisphere that are observationally more prone to blocking, i.e. the Euro-Atlantic and Pacific, are then identified and defined, with the following longitudinal limits:

Euro-Atlantic: 26.25°W – 41.25°E
Pacific: 116.25°E – 213.75°W.

A sector is then assumed to be blocked if three or more adjacent longitudes within its limits are blocked according to the previous local index definition ("sector blocking").

These criteria are sufficient to define a local (in time and space) block-like pattern. True synoptic blocking (i.e. in the sense of Rex 1950a, b) however requires a certain time-persistence of the event. Consequently, a further time requirement has to be added to the sector blocking definition. This requirement was arbitrarily chosen to reject any sector blocking lasting less than five days, again consistent with TM. The rejection of short blocks is best performed after the removal of any index-generated noise, mostly given by ″threshold-edge events″, which intermittently may or may not fulfill the requirements of the index. A number of such events were found, requiring special tapering of the time sequence. In summary, the tapering-filtering algorithm used consisted of the following two steps applied in sequence:

1. When two successive days are considered blocked by the index in a sector and are followed by a non-blocked day and then by two more successive blocked days, the whole event is considered as a five-day long block (implicitly assuming that the "hole" was due to an index failure). An analogous tapering criterion is applied in the cases of a single non-blocked day preceded (followed) by four blocked days and followed (preceded) by a single blocked day.
2. All episodes of blocking shorter than five days are excluded from subsequent analysis.

The local (in longitude) definition of the index alone was, however, used to produce diagrams of blocking frequency as a function of

longitude alone and as a function of both longitude and time (in the Hovmöller diagram format). The sector blocking definition is somewhat more synoptically based and is then used for producing distributions of blocking duration, seasonal cycles and mean blocking anomalies (blocking signatures).

3 Background

A number of blocking diagnostic techniques, including the one described, have been applied to the results of numerical weather prediction (NWP) models, as for example in TM, Tracton et al. (1989), Tracton (1990), Miyakoda and Sirutis (1990), Brankovic and Ferranti (1992), Anderson (1993), Tibaldi et al. (1994) and Tibaldi at al. (1995), where the diagnostic was used both as a tool for model validation and as mean for investigating the nature of the blocking process. Nevertheless, a comparatively smaller number of papers also deals with blocking in climate models, examples being Blackmon et al. (1986), Mullen (1986), Sausen et al. (1993), May (1994) and Tibaldi et al. (1997, hereafter TEA97). The present study follows the main outline (and represents an extension) of TEA97, where a comparison of blocking in different versions of the ECHAM3 model was made. The main conclusions arrived at by TEA97 will be reviewed briefly since, as it will become clearer later, some of the behaviour of the AMIP models in modelling blocking can be better understood in the framework of ideas set in TEA97.

First of all, TEA97 observed that while an increase of model resolution is sufficient to improve the simulation of blocking in the Euro-Atlantic (E-A) sector, the presence of more realistic variability in the oceanic lower boundary condition is necessary (as in an integration with observed rather than climatological SSTs), in addition to the higher resolution, to enhance the realism of the simulation in the Pacific sector (PAC). This suggests that blocking in the two sectors may be the result of partially different dynamical processes. Euro-Atlantic blocking appears to be more the product of nonlinear internal dynamics, whereas Pacific blocking seems to be more influenced by the interaction of the atmosphere with the underlying sea surface. This latter fact was also found to be consistent with the work by Ferranti et al. (1994) which showed the sensitivity of Pacific blocking to the specification of tropical SSTs.

Turning attention to blocking signature diagrams, i.e. blocked minus zonal composite maps (analogous to Fig. 8, see later), TEA97 found evidence that the main problem of models' representation of sector blocking patterns is connected with their inability to produce localised signatures. Additional, weaker, patterns were evident in model output and in some cases were reminiscent of the classical Wallace and Gutzler (1981) teleconnection patterns.

A difference of behaviour in the two sectors was also found in the frequency distribution of blocking duration. There was a tendency of lower resolution integrations to produce shorter blocks than-observed in the E-A, while higher resolution integrations appeared to be less prone to this error. The situation was shown to be different in the Pacific sector, where the performances of the model at different resolutions were comparable. Additionally, the use of observed SSTs as opposed to climatology did not appear to influence model blocking lifetimes. Confirmation of this behaviour was found by Déqué and Piedelièvre (1995) in the ARPEGE model of Météo France. In ARPEGE, low-frequency variance was found to be dependent on resolution in the Atlantic but not in the Pacific region.

From this above, evidence emerges that the nature of the blocking phenomenon is different in the Euro-Atlantic and Pacific sectors. The two sectors are characterised not only by a different sensitivity of blocking frequencies towards SST model forcing, but also by different seasonal variations and by different sensitivities of the distribution of blocking lifetimes to model resolution.

Before turning to the diagnosis of the AMIP models' performances, it is first useful to summarise the main features of observed blocking climatology, as they emerge from the NMC/ECMWF analyses. In Fig. 2b the Hovmöller diagram of the seasonal cycle of observed blocking frequency as a function of longitude and month is shown. The December–January–February (DJF) blocking frequency as a function of longitude is contained in Fig. 2a. Figure 2c,d shows the seasonal cycles of blocking in the two main sectors (thick lines, sectors defined in Sect. 2). In the three latter diagrams an attempt is also made to estimate the degree of interannual variability in blocking frequency.

The average observed frequency as a function of longitude (Fig. 2a) and the seasonal cycle of sector blocking frequency in the E-A (Fig. 2c) and PAC (Fig. 2d) were computed over eight and staggered, partially overlapping, periods of ten years (the eight thin lines in each diagram) spanning the entire dataset of analysed data available, ranging from December 1949 to February 1994. The diagrams show significant interdecadal variability, quantified by the grey band representing one standard deviation computed among the eight ten-year means. For direct comparison with model output, nevertheless, only the 10-y AMIP reference observed period has been used.

The sampling problem connected with the evaluation of blocking frequency in a 10-year model integration is evident from Fig. 2a, 2c and 2d. The particular choice of the 10-y period can play an important role, due to the presence of a strong interannual variability in blocking occurrence on the 5–10 y time scale, as was illustrated in TEA97 or in D'Andrea et al. (WMO 1996).

Returning to Fig. 2a,b, the two preferred blocking sectors (E-A and PAC) can be easily identified. In Fig. 2a it is also possible to observe that the interdecadal variability of blocking (the standard deviation

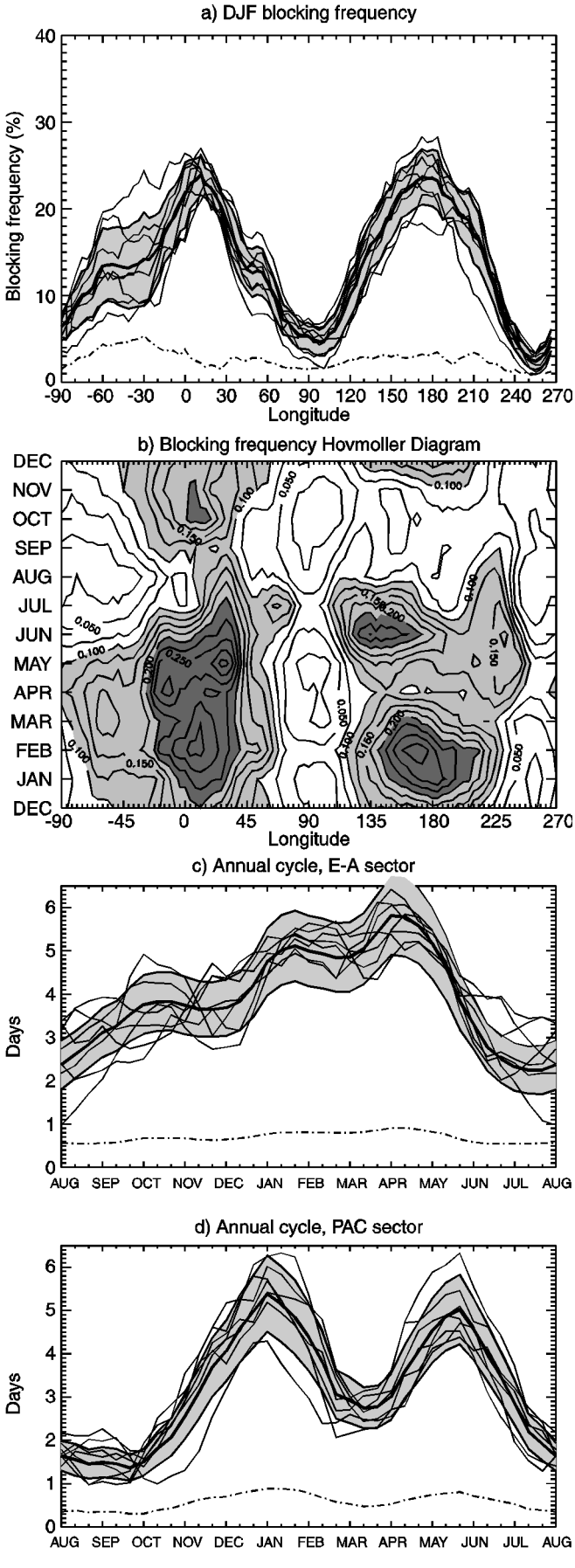

among the eight thin lines is shown by the dash-dotted line in all panels 2a, 2c and 2d) has a maximum in the western-atlantic area (around 60 °W-20 °W). It will be shown below that the models also exhibit a variety of different behaviors in this area.

The comparison between Fig. 2c and 2d shows that the two main blocking sectors are characterised by different seasonal cycles, both sectors having a maximum in spring; the Pacific also has a maximum in winter, while the Euro-Atlantic exhibits a relatively lower activity in winter. The interdecadal standard deviation (the dash-dot line) does not show any large seasonal dependence, other than the increases in correspondence with the maxima of the mean signal.

Figure 2b gives an idea of the complexity of the seasonal variations of blocking climatology in longitude. In particular, the presence of a secondary maximum of activity in the western-Atlantic (WA) region (around 50 °W) in March can be observed, together with the split of the Pacific maximum from April to July. In this period, the main maximum migrates from 180 °E to 140 °E, while a second, somewhat weaker, feature originates around 240 °E. The choice of the DJF period instead of a period of higher blocking activity (such as spring or early summer), is often made throughout this work (e.g. Fig. 2b) to facilitate the comparison with previous works, which tended to concentrate on the winter period.

Finally, Fig. 3 shows the frequency distribution of blocking duration for the two sectors, where it should be noted that a logarithmic scale is used in the frequency axes in order to illustrate the fact that the distribution displays an exponential decrease. In the two panels, a least-square interpolated straight line is superimposed, computed on the frequency of blocking duration of between 5 and 20 days. (This period has been used to minimise sampling problems.) Since the population of each bin of the observed distribution is assumed to belong to a Poisson distribution, each bin is weighted by $\sqrt{n}$, n being the observed frequency of cases with a given duration. The expected distribution, obtained with the least square fit, is also displayed with its one standard error limits (dashed). The least square fit has a correlation with the observed distribution of 0.92 in the E-A sector and of 0.93 in the PAC. Assuming 14 degrees of freedom, both of these coefficients are significant at more than the 99% confidence level.

Fig. 2a–d Observed blocking frequency during the period 1949–1994. **a** Blocking frequencies as a function of longitude for 8 partially overlapping periods of 10 y (*thin lines*). The *thick line* shows the mean value, the area within the interval of standard deviation is in *grey*. *Dash-dotted line* is the value of the standard deviation. **b** Blocking freuency Hovmöller diagram (longitudinal-seasonal). Areas higher than 10% and 20% are *shaded*. **c** As in panel **a** but for blocking episodes frequency annual cycle, expressed as average number of blocked days per 10-day-period of the year, Euro-Atlantic sector. **d** As in **c** for the Pacific sector

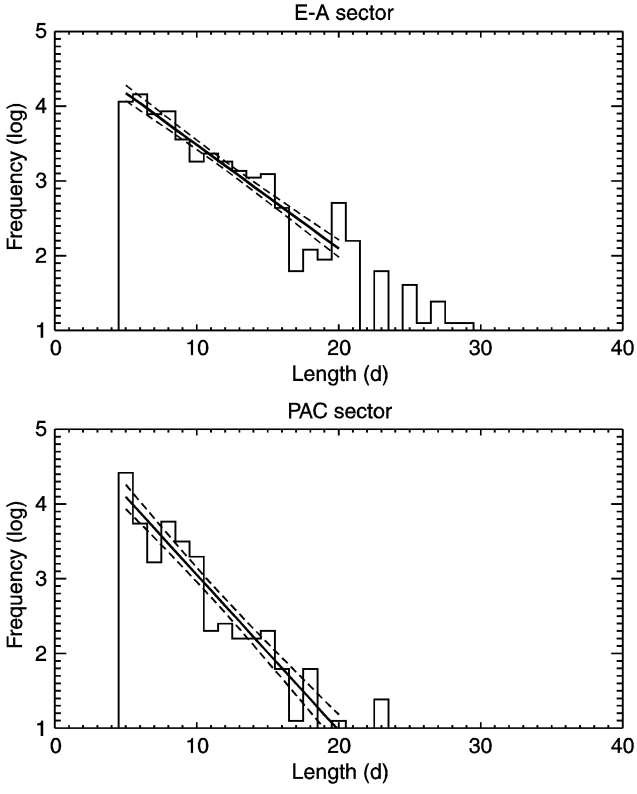

Fig. 3 Histogram of the frequency distribution of blocking length for the analysis in the two sectors (E-A sector *top*, PAC sector below). Logarithmic scale on the y-axis. The *straight line* is a least-square fit of the distribution, computed on the 5 to 20 day interval; the standard error on the least square fit is also shown (*dashed line*)

An exponential shape of the distribution of blocking duration was also found by Dole and Gordon (1983). The authors interpreted the shape of the distribution as evidence of the fact that the probability of the block to survive for $t + 1$ days is independent of t. In other words, the atmosphere (or rather the transient processes that are thought to maintain or destroy the block) does not carry any memory of the duration of the phenomenon.

4 Blocking in the AMIP integrations

4.1 Blocking frequency

In this section, the season-longitude dependence of local blocking frequency will be shown for the different models.

Figure 4, panels *a* to *r*, shows the DJF blocking frequency as a function of longitude in the analysis and different models. The wide variety of behaviour in the different models can be readily appreciated. In these diagrams, the observed blocking frequency is superimposed in grey, as the band defined by the mean 1979–88 value plus and minus one standard deviation, computed as in Fig. 2a. The main conclusion is of a general tendency to underestimate the blocking activity. There are only a few cases of model overestimation, notably in the WA region, by CSIRO, COLA, NMC and to a lesser extent by UGAMP, UKMO and NCAR, although the behaviour of the latter three models falls within the observed natural variability band. It must also be added that the WA area is the one of maximum variability of observed DJF blocking frequency, as has already been pointed out (Fig. 2a). Among the models overestimating WA blocking frequency, the case of CSIRO is different. Apart from the excessive amplitude of this peak, the model does not show much blocking activity in the more usual Euro-Atlantic sector. The peak could therefore represent a strong westward shift of Euro-Atlantic blocking. The other models mentioned, on the contrary, all show a discernible E-A peak, in addition to the WA one. Considering the 500 hPa DJF climate of the CSIRO model (see the Appendix, Fig. A1d), it can be noticed that there is an excessive orographic wave over Greenland, which causes a noisy pattern in the high latitudes (60–80 °N) of the WA blocking maximum sector (20–60 °W). The excessive blocking frequency may therefore partially be a result of a bad simulation of the Greenland ridge, in turn caused by the wrong angle with which the large-scale flow impinges the Greenland orography, much more W-to-E rather than SSW-to-NNE (compare Fig. A1d with Fig. A1a). This could well cause an undesirable response in the blocking index. It should, however, be pointed out that the spuriously high blocking peak at 40–50 °W is borne out by an equally spurious maximum of low-frequency variability in the same area (Fig. A2d).

Turning our attention now to the more complex behaviour of blocking frequency in longitude and seasonal phase, the Hovmöller diagrams for all AMIP models can be considered (Fig. 5 *a*–*r*). Fig. 5 *a* refers to the analysis for the 1979–88 period. (Note that the analysis is slightly different from that in Fig. 2b, which refers to the much longer period 1950–94.) The wide range of behaviour seen in Fig. 4 is again visible.

Since the DJF period has already been analysed, attention can be focused firstly on the double shape (split) of the Pacific maximum in the extended spring period April to July. Some models, notably NCAR and COLA, provide a good reproduction of both shape and phase of the maxima, together with a satisfactory amplitude. CCC and DERF/GFDL have a good location and shape, but a slightly underestimated amplitude. Other models (NMC, UGAMP, ECHAM UKMO) reproduce a pattern that resembles the split peak, but they miss the location, shifting it in time or (more rarely) longitude. CSIRO is somewhat a special case, showing a well-placed Pacific maximum, notwithstanding the problems evident at 90 °E, probably due to difficulties with the definition of the 500 hPa GPH field

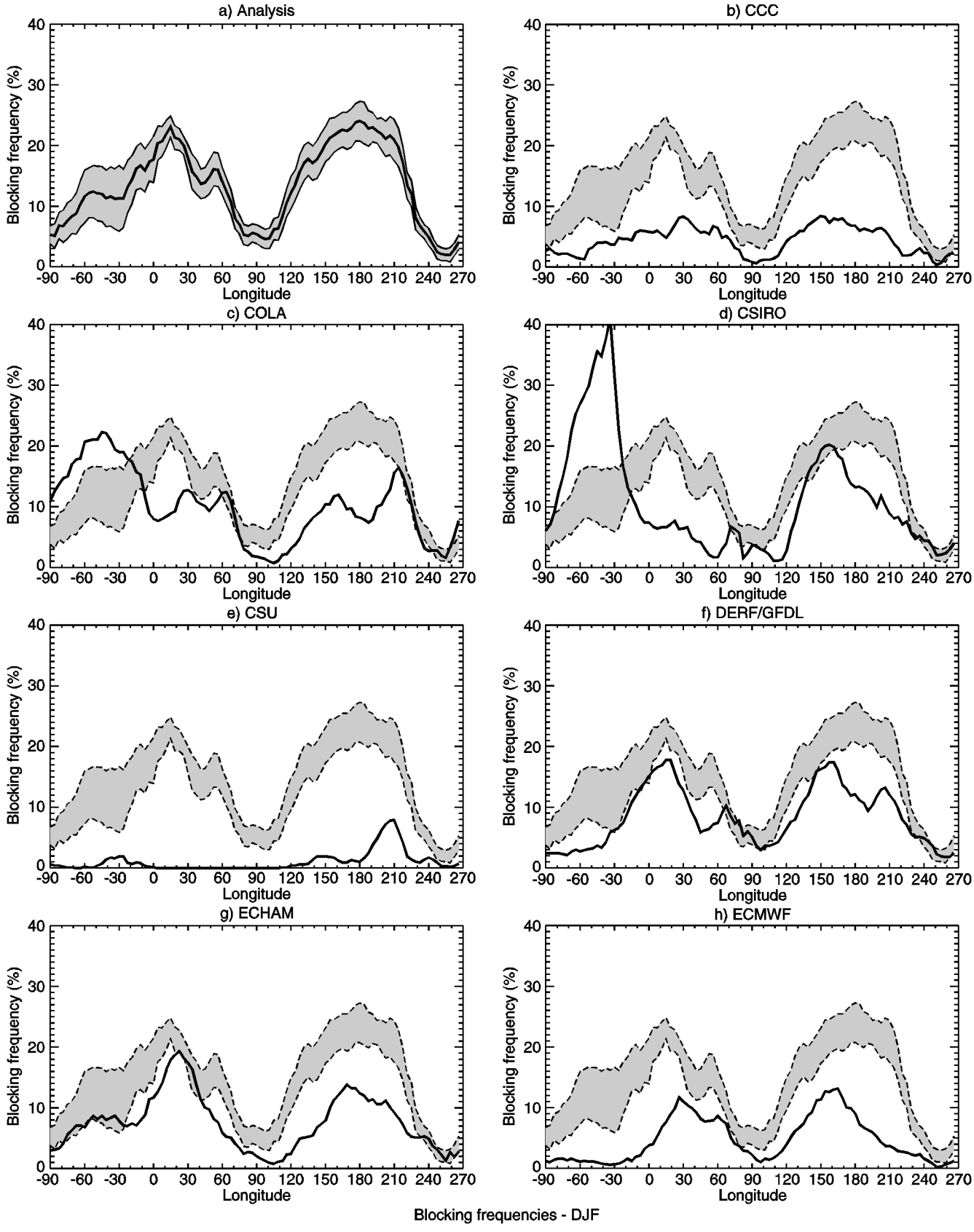

Fig. 4a–r Longitudinal blocking frequencies. In **a** the observed value is reported with it standard deviation in *grey* (see also Fig. 2). In **b** to **r** the *black line* refers to the AMIP model output, the *grey area to* the observed value

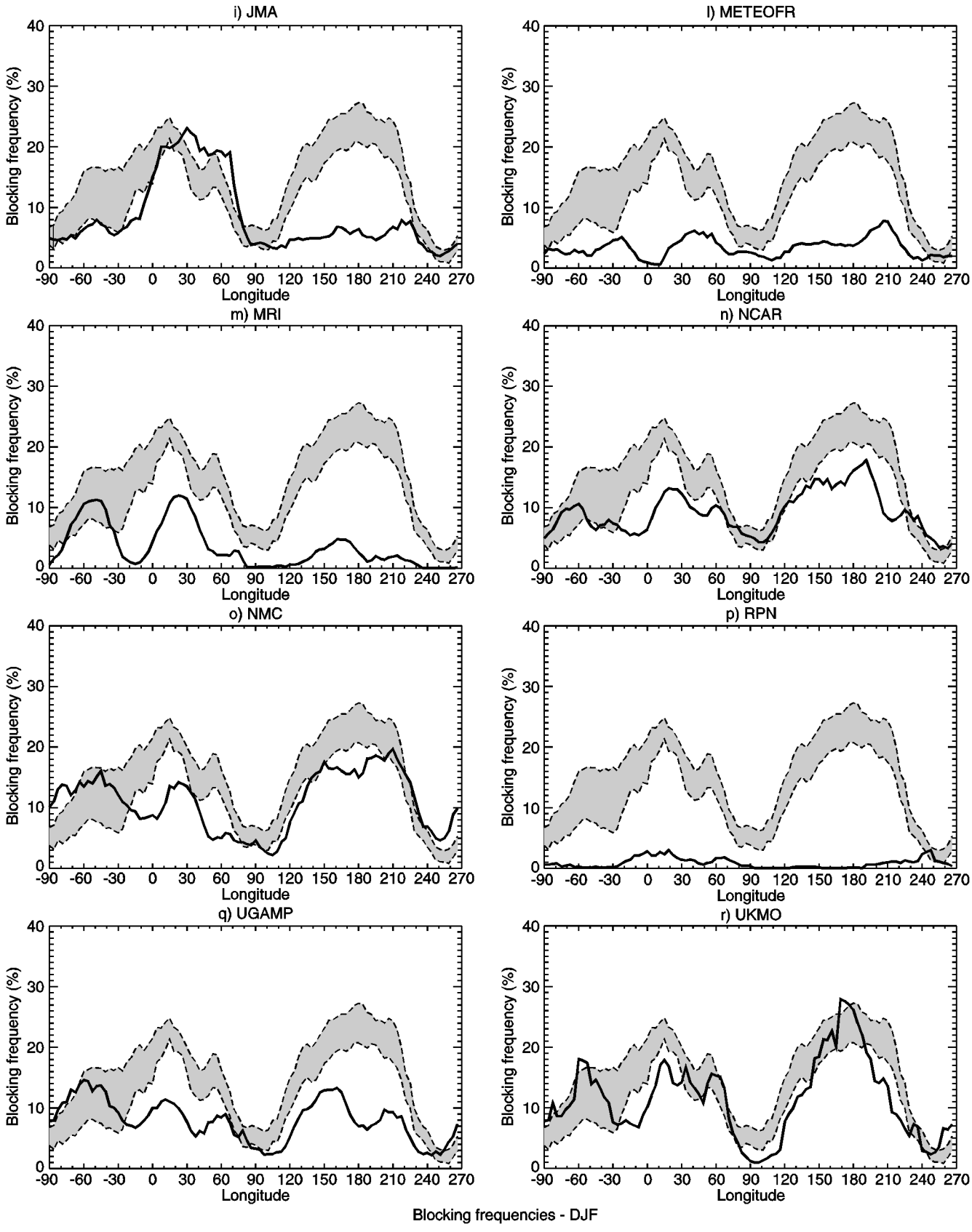

Fig. 4 (continued)

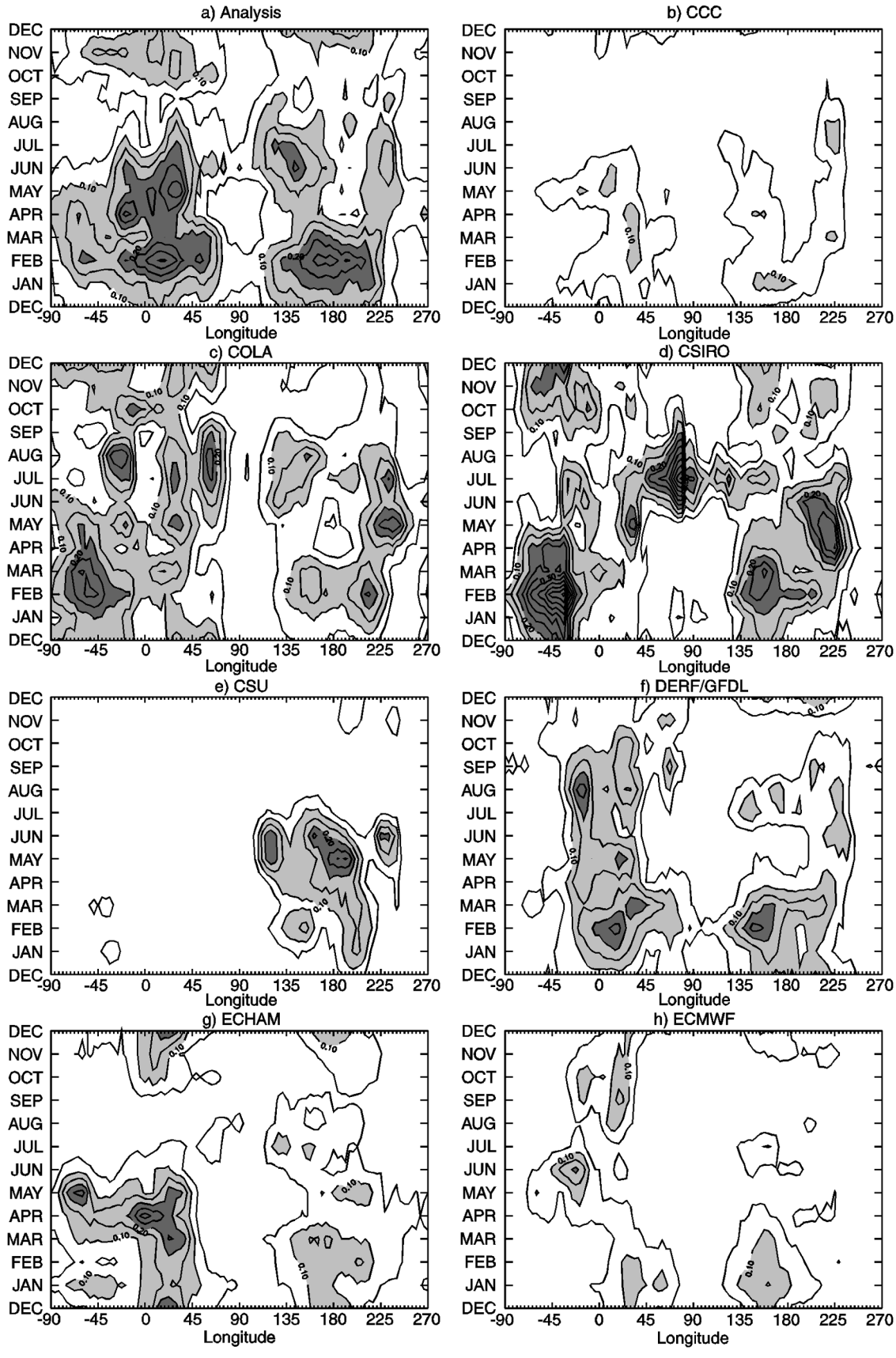

Fig. 5a–r Hovmöller diagrams of annual cycle of observed blocking frequency. **a** for observed values 1979–1988. **b** to **r** for participating models. Areas higher than 10% and 20% are *shaded*

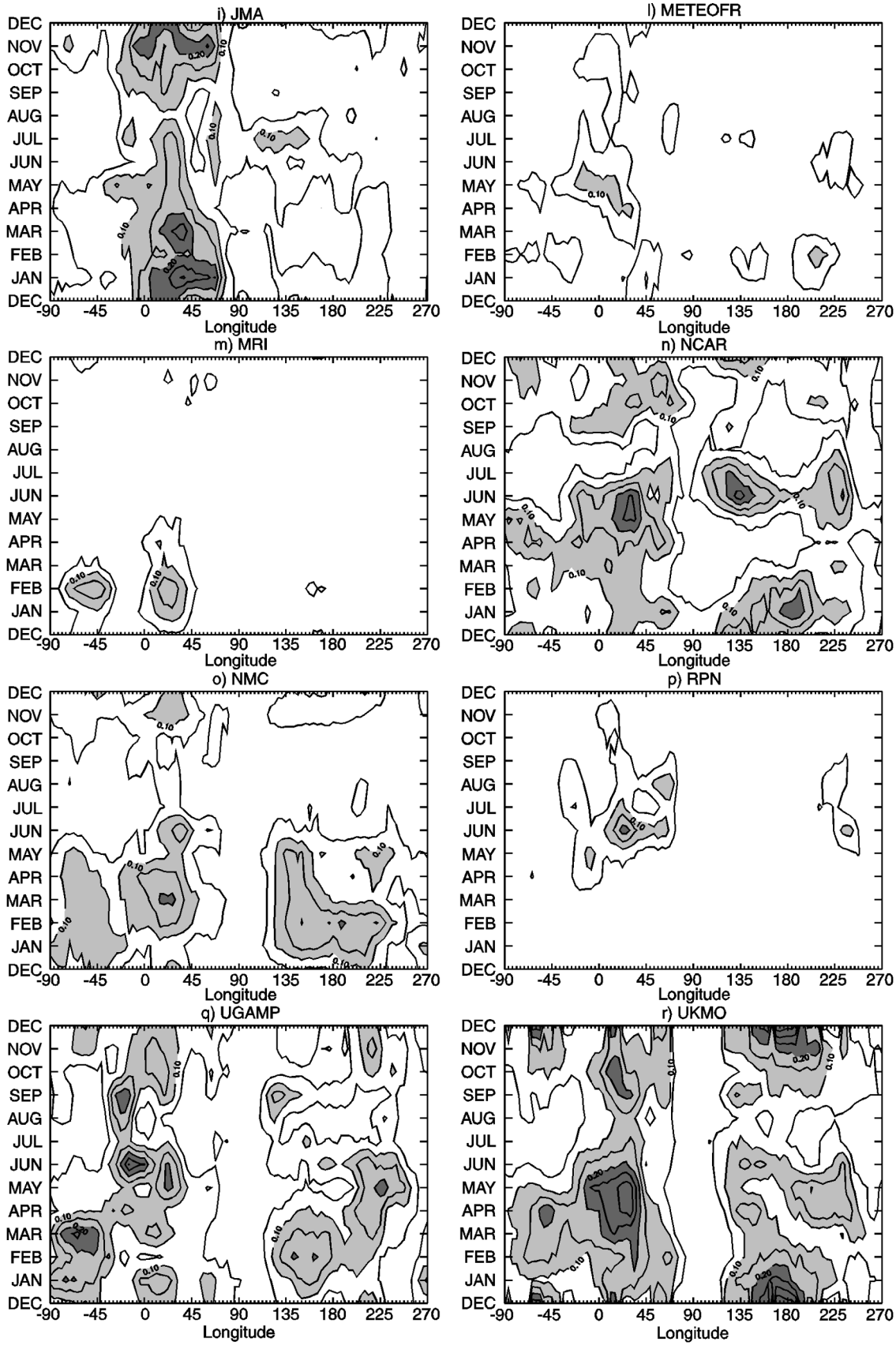

Fig. 5 (continued)

in the Himalayan region (see also Fig. A1d in the Appendix).

The February–March–April secondary maximum in the western-Atlantic region (WA) is also worthy of attention. Some models reproduce it (shifted at times in space and/or time) and some miss it. COLA has a maximum in the WA, but it is too extended and may be better interpreted as a displacement of the main Euro-Atlantic peak. UKMO has a good simulation of the maximum and of its amplitude, spatial placement and extension in time being very realistic. CSIRO is again peculiar, with an extremely overestimated maximum, also clearly visible in Fig. 4d. NMC has a plateau in the WA which extends too long in time. NCAR and ECHAM both shift the WA maximum towards the April–May period. Other models also show a WA relative maximum in March–April–May, although generally with too low an amplitude, which makes it difficult to identify patterns clearly; this is the case with ECMWF, METEOFR, JMA, CCC and DERF/GFDL. Some other models show a longitude-time pattern in which it is difficult to recognise observed features, as in the case of CSU, MRI, and RPN.

The models characterised by a generally poor representation of the Fig. 5a Hovmöller diagram also show a poor reproduction of the DJF blocking frequency. It should be pointed out that MRI and CSU are the lowest resolution models of the whole set, and that both are gridpoint models rather than spectral. Interesting and opposite counter-examples to this tendency are represented by RPN and UKMO models. The first is spectral T63 (which is a comparatively high resolution, although the model output was provided at T21) and shows a poor performance, while the second is a gridpoint model, but with a resolution ($2.5^\circ \times 3.75^\circ$) higher than that of MRI and CSU and its performance is very good.

The case of JMA is peculiar, since the model provides a very well represented E-A blocking during the DJF period (although the maximum is shifted eastward). However, this good performance is limited to DJF, with the model performing much less satisfactorily during the important observed spring maximum and in the PAC sector in general. The spring maximum problem is visible both in the JMA Hovmöller diagram (Fig. 4i) and also in the JMA E-A sector annual cycle (Fig. 6i, see later).

4.2 Sector blocking episodes

The climatology of "blocking episodes" (i.e. sequences of more than four sequentially blocked days, as selected by the index and by the tapering-filtering algorithm described in Sect. 2) has been analysed in the two Euro-Atlantic and Pacific sectors. In this section, the blocking seasonal cycle (Fig. 6) and lifetime distribution (Fig. 7) will be assessed.

The general model underestimation of blocking frequency shown in Sect. 4.1 was diagnosed making use of the local and instantaneous blocking index definition. Since our attention will now be restricted to sector-blocking episodes, it is necessary to verify whether that conclusion still carries over. Table 2 gives a list of the total number of DJF days belonging to a blocking episode for both sectors, and demonstrates that model blocking underestimation is not affected by the elimination of short blocks from the sample.

Figure 6 illustrates the seasonal cycle of E-A sector blocking. The diagrams are obtained as percentage of blocked days for any ten-day-period of the year. Again the large model-to-model variability of behaviour is evident. A number of models have recognisable seasonal cycles which, in some cases, show a good correspondence with observations (ECHAM, CCC, CSIRO). In other cases models tend to have blocking earlier in the year (JMA, NCAR, NMC, UGAMP, METEOFR, UKMO) and in one case later in the year (DERF/GFDL). Note that the observed seasonal cycle is repeated (dashed) in all panels. For some models, the comparison with observations is made particularly difficult by the generally low-level of model blocking activity. The case of CCC is interesting since the model has a seasonal cycle in good agreement with observations, although with a much reduced amplitude.

The seasonal cycle in the PAC sector is not shown, but the interested reader can find the figures referring to the totality of the models in D'Andrea et al. (WMO 1996). Some models show a very good performance in the PAC sector, like NMC, NCAR, COLA, DERF/GFDL and CSIRO, while others have an acceptable variation but with a reduced amplitude; this is the case of METEOFR and JMA and to a lesser extent of MRI and CCC. Many of these features can also be seen in the Hovmöller diagrams in Fig. 5.

In D'Andrea et al. (WMO 1996) the distributions of blocking duration are reported for every model. Here only some considerations will be made on the lifetime distributions. Some models show this in a remarkably accurate way. However, it should be noted that although there are some models that tend to produce shorter blocks than observed, no model shows a tendency to produce longer blocks. Models showing the largest departures from the observed distribution are in general those with very few blocking cases anyway, and consequently the distribution is highly prone to sampling errors (MRI, RPN).

Another way to compare the blocking duration distributions among models is by verifying their expected exponential shape (as described in Sect. 3), checking its first and second order moments. In Table 3 the mean (μ) and standard deviation (σ) of the distribution of each model are listed for both sectors, and were computed over the restricted period ranging from 5 to 20 days. It is again confirmed by the mean durations that the

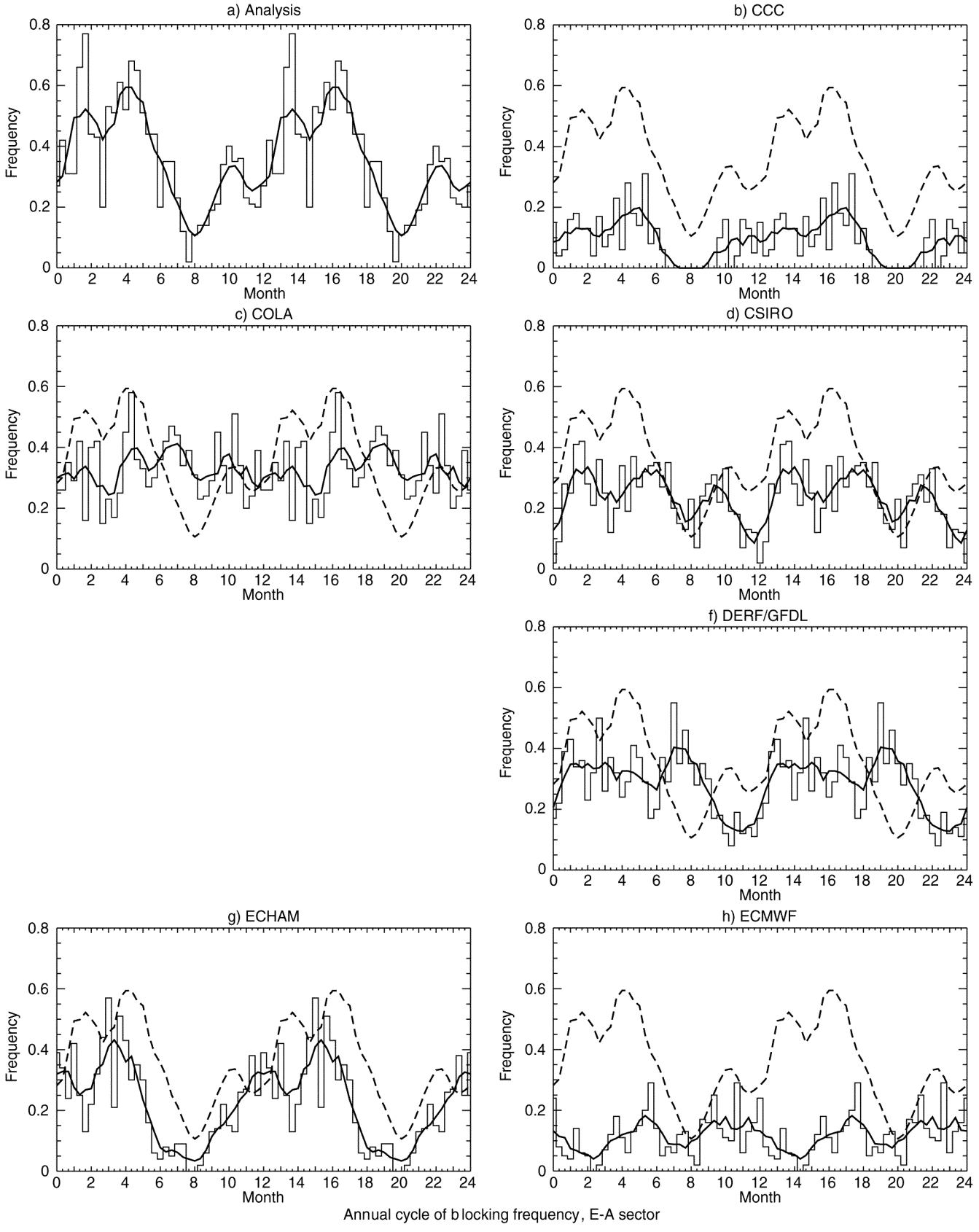

Fig. 6a–r Annual cycle of blocking frequency in the Euro-Atlantic sector, expressed as the average fraction of blocked days per ten-day period of the year. In the time axis two years are shown for visualisation purposes. The *continuous line* is a polynomial interpolation. The *dashed line* in **b** to **r** refers to the observed data. **e** is incomplete due to an insufficient number of blocking cases for CSU model

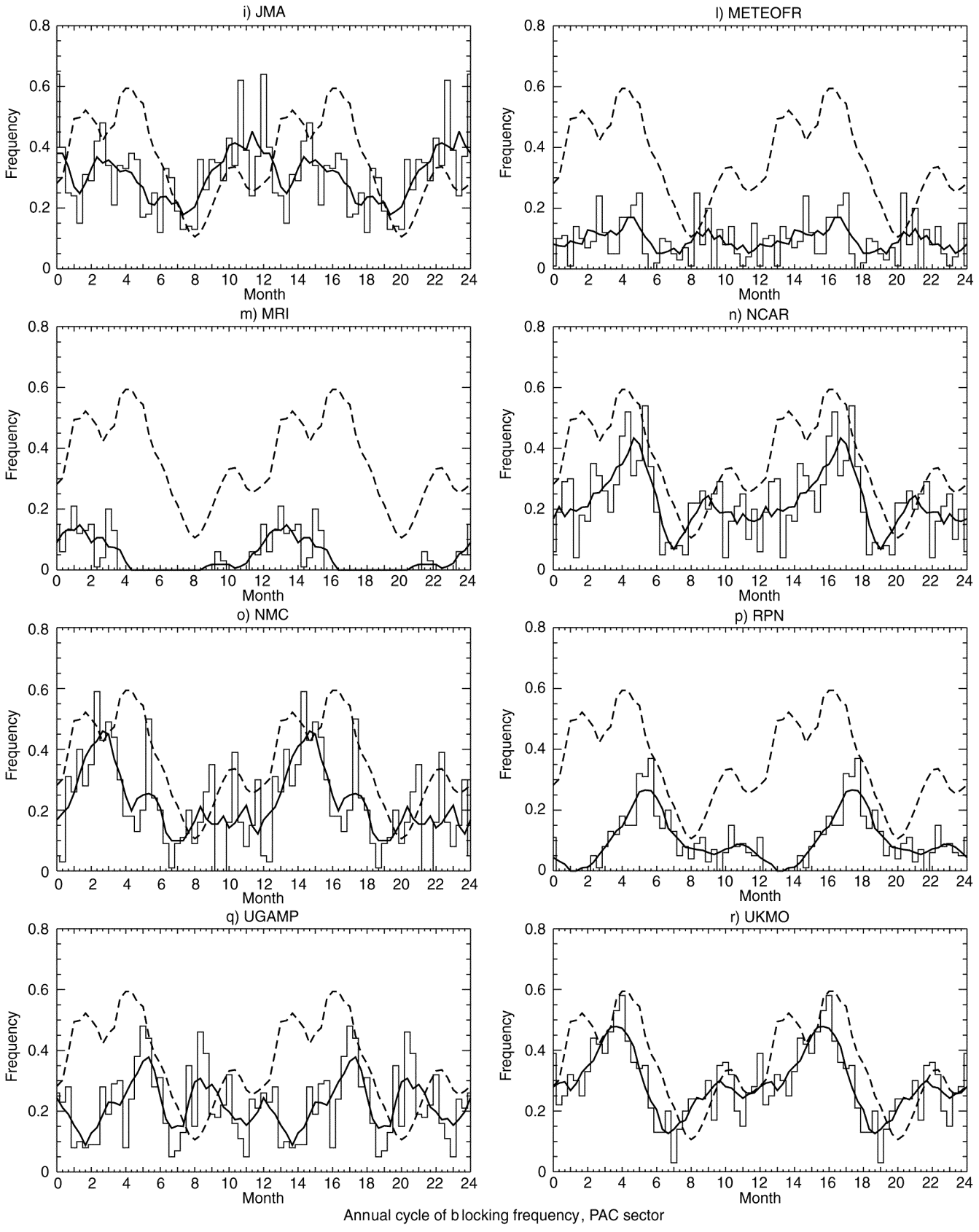

Fig. 6 (continued)

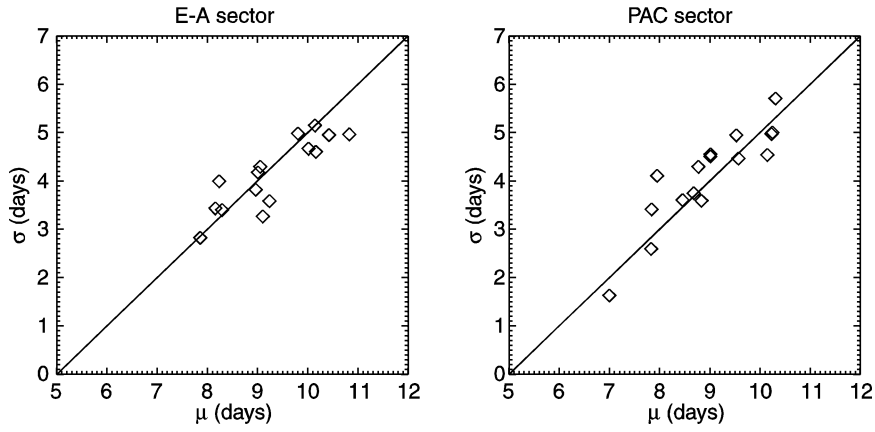

Fig. 7 Scatter plot of mean and standard deviation of the distribution of frequency of blocked days, for the E-A (*left*) and PAC sector (*right*). The straight line is the diagonal of the quadrant. Refer to Table 3 to identify the single models. CSU is not shown in the E-A sector diagram

Table 2 Number of days belonging to a blocking episode in the Euro-Atlantic and Pacific sectors for the analysis and for the different models. Note that not all the models consider leap years

Model	E-A blocked days	PAC blocked days	Total number of DJF days
Analysis	331	450	903
CCC	105	17	902
COLA	263	166	902
CSIRO	179	288	903
CSU	–	–	903
DERF/GFDL	227	313	903
ECHAM	267	214	900
ECMWF	103	162	903
JMA	299	94	900
METEOFR	67	106	903
MRI	107	51	903
NCAR	162	331	900
NMC	149	247	722
RPN	32	9	903
UGAMP	176	238	903
UKMO	270	397	903

Table 3 Mean (μ) and standard deviation (σ), expressed in days, of the distribution of frequency of blocking duration in the two sectors, computed on the period 5 to 20 days

Model	μ	σ	μ	σ
	Euro-Atlantic		Pacific	
Analysis	10.8	4.9	10.2	5.0
CCC	7.9	2.8	7.8	3.4
COLA	10.0	4.7	8.8	3.6
CSIRO	9.0	4.2	10.1	4.5
CSU	–	–	8.7	3.7
GFDL/DERF	10.2	4.6	10.2	5.0
ECHAM	9.0	3.8	9.0	4.5
ECMWF	8.2	4.0	8.5	3.6
JMA	9.8	5.0	7.9	4.1
METEOFR	8.2	3.4	7.8	2.6
MRI	9.2	3.6	9.6	4.5
NCAR	10.1	5.1	8.8	4.3
NMC	9.1	3.3	9.5	4.9
RPN	8.3	3.4	7.0	1.6
UGAMP	9.0	4.3	9.0	4.5
UKMO	10.4	4.9	10.3	5.7

models have a general tendency towards shorter blocks. To test the fit of the distributions to the exponential form, a χ^2 test was attempted. Unfortunately, this approach was found to be problematic due to sampling error at longer lifetimes. A better approach is to check the expected relationship between the mean and the standard deviation of the exponential distribution. It can be shown that, for an exponential distribution, $\mu = \sigma = 1/\lambda$, where λ is defined by the probability distribution $P(t) = \lambda e^{-\lambda t}$. In the case of the distribution of blocking lifetimes, since the distribution is truncated at 5 days of minimum duration, it can be easily shown that the relation between the mean and standard deviation must be replaced by $\sigma = \mu - 5$. In Fig. 7, μ and σ for the different models are shown on a scatter-plot. The models all lie close to the straight line $\sigma = \mu - 5$, consistent with having an exponential distribution. This means that the fact that the probability of a block lasting from n to $n + 1$ days is independent of n (see Sect. 3). This property of the blocking duration is well modelled by the GCMs, irrespective of their tendency towards shorter blocks.

The model tendency towards shorter blocks was also observed in TEA97, especially for the lower resolution runs of the ECHAM model. This failure was less evident in the higher resolution integrations and in the E-A sector for that model. In TEA97, this effect was tentatively attributed to the lack of eddy activity in lower resolution models, providing therefore a reduced eddy straining effect. The eddy straining effect is considered to be an important process for blocking maintenance, particularly in connection with the E-A blocking and the Atlantic storm track (Green 1977; Shutts 1983; Hoskins et al. 1983; Mak 1990). The lack

of long-lived blocks is confirmed to be a common feature of most analysed models, as well as the overall underestimation of blocking frequency, which is far more evident.

4.3 Blocking signatures

Blocking signatures (Fig. 8) are obtained by subtracting from the composite field of all the days belonging to a

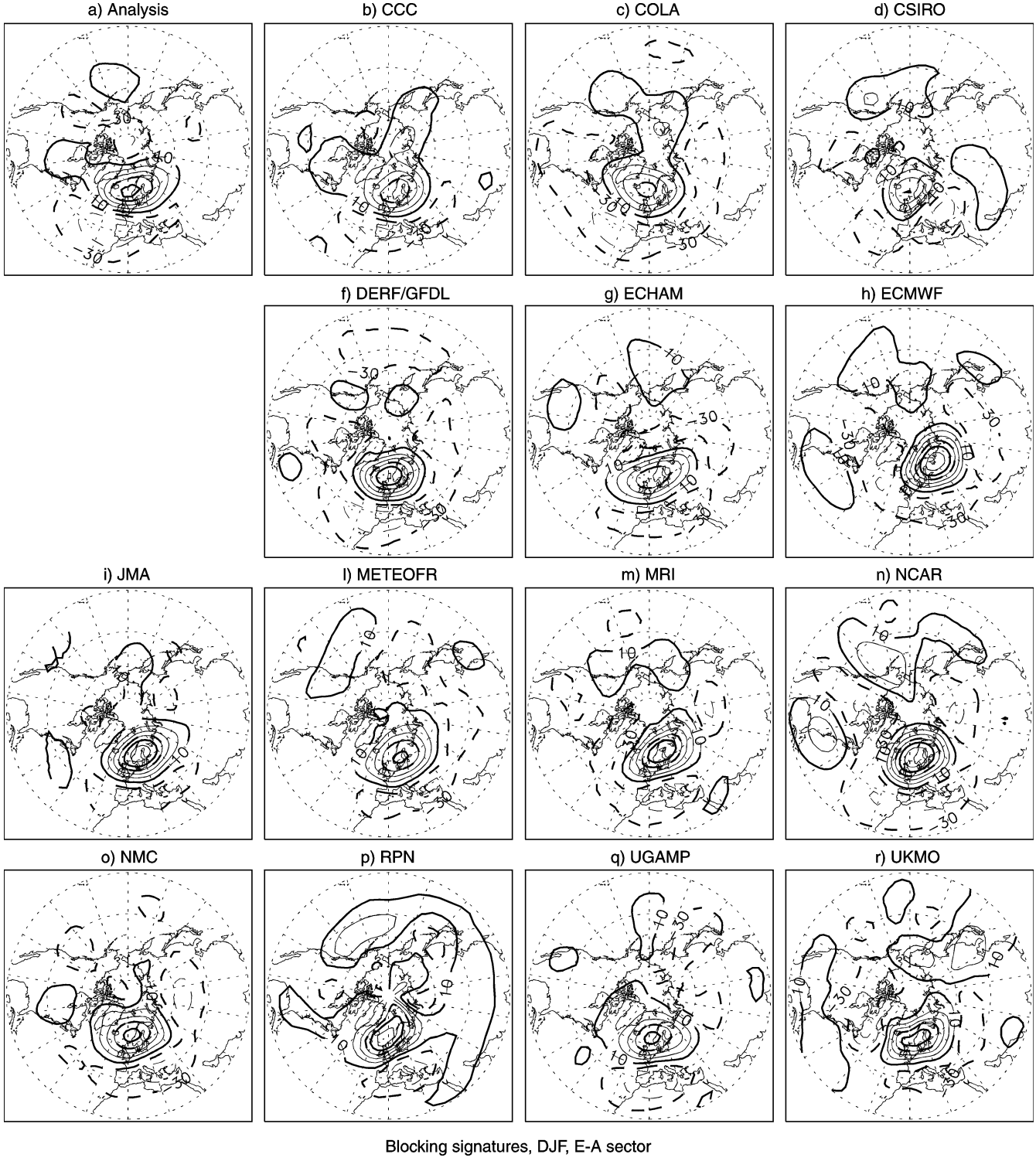

Fig. 8a–r "Blocking signature" (i.e. the difference of blocked and non-blocked composite maps) of the Euro-Atlantic blocking in the DJF period. Contour interval 20 m, *negative* contours *dashed* (Table 2 shows the number of blocked days for each model). **e** is missing due to an insufficient number of blocking cases for the CSU model

sector blocking episode the composite field of the remaining days. In other words they represent the difference between the blocked and non-blocked (zonal) ensemble means. This analysis will be limited to the DJF period.

This diagnostic tool is particularly useful to assess the average location, shape and intensity of the blocking highs and lows. The information about the longitudinal location of the sector blocking maximum was already provided by the DJF blocking frequency diagrams described in Sect. 4.1 (Fig. 6). Those results are confirmed by the longitudinal location of the blocking dipoles evident in Fig. 8. Signature diagrams however provide additional information on the average blocking intensity (measured by the amplitude of the blocking high) as produced by models, irrespective of how often they produce blocking and of its exact longitudinal location. Sector blocking can be synoptically considered as a local weather regime (e.g. Vautard 1990), which justifies the procedure of subtracting blocked minus zonal composite maps, rather than computing traditional anomaly maps.

The location of the maximum of the blocking high in the E-A tends to be shifted toward the east in a number of models (CCC, ECMWF, JMA, METEOFR, MRI, NCAR, UKMO), while in the PAC sector there is no such tendency and both eastward and westward shifts occur. In the E-A sector, METEOFR, NMC and UGAMP reproduce the exact blocking high amplitude, while CCC, ECHAM and COLA slightly underestimate it. Other models heavily overestimate the amplitude: this is the case of JMA and NCAR and, somewhat less strongly, of DERF/GFDL and MRI. RPN also overestimates the amplitude, but for this model (as for others) the relevance of this result is weakened by the paucity of blocking cases produced (refer to Table 2 for the number of blocked days).

Another feature visible in many panels of Fig. 8 is the presence of wave train-like structures, some of which closely resemble the PNA pattern. Wave train-like patterns are visible in ECHAM, ECMWF, METEOFR, MRI, NCAR and somewhat less clearly in JMA and DERF/GFDL. It must be added that a similar feature (albeit weaker in intensity) is also present in the analysis panel. In TEA97 this feature was also identified in the same 10-y analysed blocking signature, but this was shown to be due to sampling problems, as longer period averaging on observed data (43 y) tended to eliminate such structures and showed isolated blocking dipoles. Some models (UGAMP, RPN, METEOFR, JMA) also tend to show the presence of a wave number 5 pattern. In the Pacific sector (not shown, see D'Andrea et al. WMO 1996) CCC, COLA, CSIRO, METEOFR, NMC and UGAMP all reproduce the blocking high amplitude reasonably, although CCC has a very small overall number of blocks. ECHAM, on the other hand, reproduces the shape of the blocking high, but with an overestimated intensity.

5 Model systematic errors and blocking

From previous studies, it is implied that the relationship between model systematic error (SE) and blocking is particularly strong in the case of NWP models with resolution comparable to those analysed in the present work, for which SEs often have the shape of a reverse blocking pattern. In the case of longer integrations, as in climate models, this relationship appears to be somewhat less clear. In the intermediate case of a large ensemble of 60-day forecasts performed with the NMC-MRF model (USA-National Meteorological Center, Medium Range Forecasting model), Anderson (1993) found that the prediction shows a rapid decrease in the ability to reproduce blocking during the first days of a forecast, reaching a minimum around day ten. During the later stages of the forecast, however, the model recovers and drifts towards a more stable situation of higher (albeit still lower than observed) frequency of occurrence of blocking episodes. This can be then considered the model's own blocking climatology.

In Fig. 9, the 500 hPa geopotential height systematic error (SE) for the DJF period is shown for every model, computed simply as the difference between the model mean winter field and the observed mean field. Focusing attention on COLA, CSIRO, NMC, UGAMP and UKMO, it can be observed that all these models show a remarkable positive anomaly over Greenland and Hudson's Bay. These five models were also shown in Sect. 4.1 to have a tendency to overestimate WA blocking, which was defined as taking place exactly in the area of this anomalous error. Moreover, the positive anomaly in the WA is also accompanied by a low immediately to the southeast of it, very much resembling a blocking signature, although rotated slightly counterclockwise. The presence of the accompanying negative anomaly is not surprising, due to the strength of the Icelandic-Azores seesaw, or of the North Atlantic Oscillation (NAO), even if the pattern present in these SE maps is somewhat shifted to the northwest with respect to the classical NAO pattern.

In order to assess to what extent it is possible to ascribe the systematic error to the overestimation of blocking in the area, the SE has been computed excluding the days identified as blocked by the index in the WA sector from the composite of the model 500 hPa daily maps. The sector longitudinal limits were chosen to vary somewhat from model to model, to include the WA peak as it appears in the panels of Figs. 4 or 5. In Table 4, the sector limits chosen are listed for each model. The NCAR model integration was also included for completeness in this assessment because it also shows a notable WA peak (panel 4n), although its SE does not show a similar signature.

The results of these "zonal only" SE computations are shown in Fig. 10. It can be seen that the SE patterns are essentially unchanged everywhere, other than in the

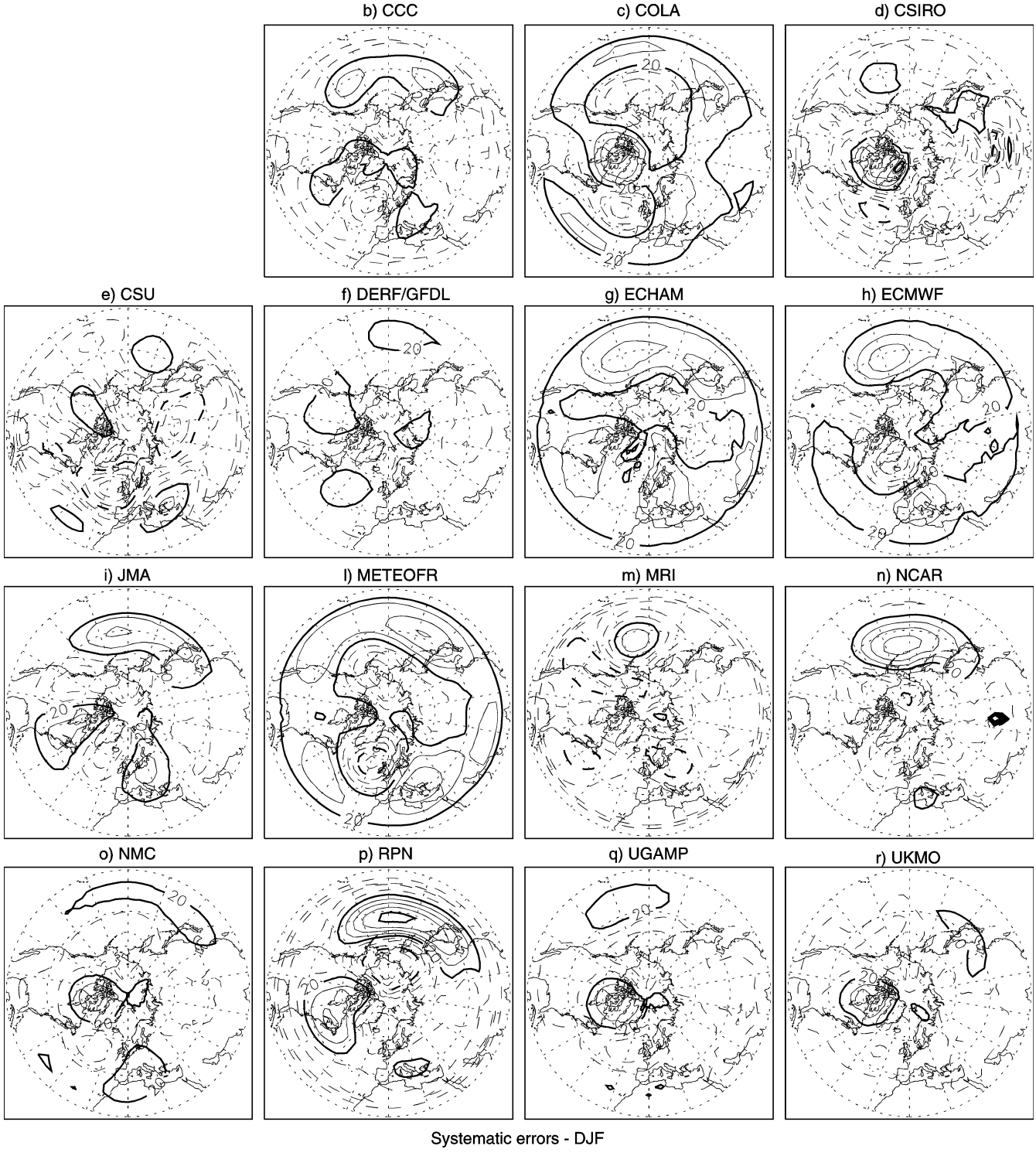

Fig. 9b–r Systematic error of the 500 hPa geopotential Height for the various models in the DJF period. The systematic error is defined as the difference of the composite modelled and observed map. Contour every 20 m, *negative* contours *dashed*

WA sector. In the WA, the dipole anomaly amplitude is slightly reduced in all models (except NCAR). The negative lobe of the dipole anomaly in the "zonal only" SE maps is also shifted slightly farther to the east, particularly for the UGAMP and UKMO models. The results for NCAR, not surprisingly, do not show any appreciable difference.

It can be concluded therefore that the removal of the excessive blocking activity in the WA sector does not substantially reduce the systematic error in the area.

Table 4 Longitudinal limits chosen for the West Atlantic sector in the models that show a high frequency of blocking in this area

Model	Western limit	Eastern limit
COLA	71 °W	11 °W
CSIRO	86 °W	4 °W
NCAR	86 °W	15 °W
NMC	90 °W	22 °W
UGAMP	86 °W	22 °W
UKMO	75 °W	30 °W

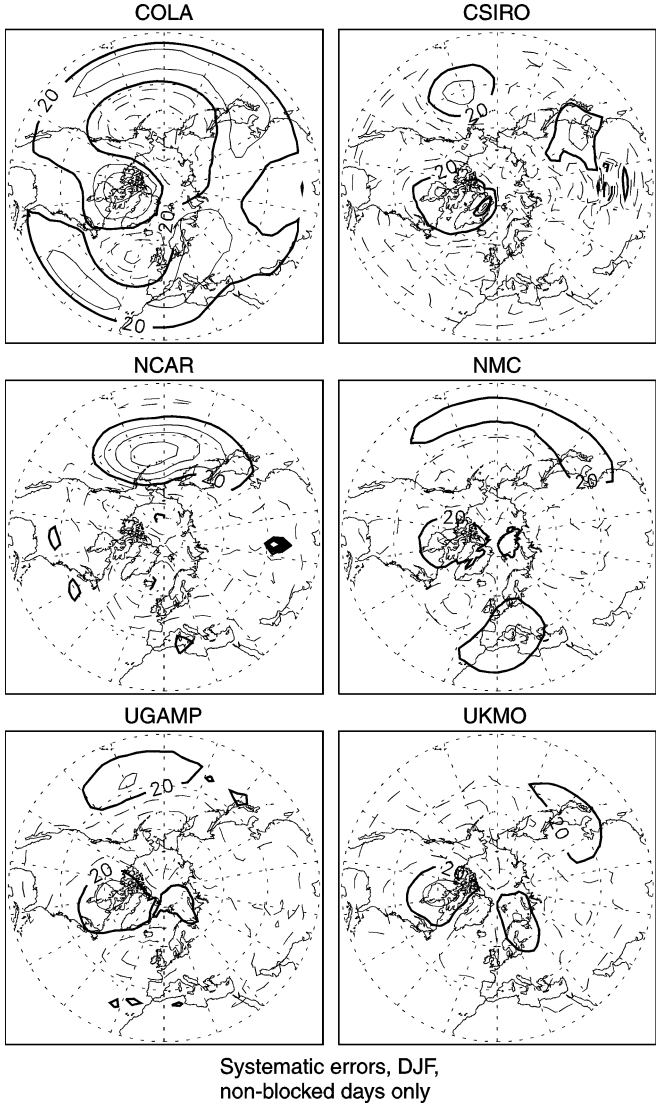

Fig. 10 "Zonal" systematic error of the West-Atlantic area in DJF, i.e. the difference between the modelled composite map of all the non-blocked days and the observed DJF composite map. Contour every 40 m, *negative* contours *dashed*

Conversely, from these maps it can be inferred that, due to the presence of this error, more blocking episodes are spuriously produced by some models in the WA area. Five of the models interested with this problem show an overestimated orographic ridge over Greenland (on the left-hand side of the jet exit over the American continent) and an underestimated Icelandic low downstream of it. This behaviour is reflected in a E-W oriented wave-like-pattern evident in the SE maps, particularly evident for UGAMP and UKMO (see Fig. 10). The evidence of the excessive Greenland ridge is also visible in the full-field mean DJF maps, shown in Figs. A1c, A1d, A1n, A1o, A1q and A1r. Moreover, in the low-frequency variability fields (panels *c*, *d*, *n*, *o*, *q*, and *r* of Fig. A2) a spurious maximum of low-frequency variability in the same area is also visible.

6 Discussion and conclusions

The models considered in this comparison span a wide range of modelling techniques usually employed in GCMs: vertical (sigma or hybrid) and horizontal (grid-point or spectral with triangular or rhomboidal truncation) discretisation, not to mention the variety of physical parametrizations. It is therefore not surprising that they show a large variety of behaviour as far as blocking representation is concerned. This is readily apparent in Fig. 11, showing the DJF blocking frequencies as a function of longitude for all models on the same panel. This variety of model behaviour is reflected in a number of indicators, notably in the longitude-time annual cycle diagrams of Fig. 5, from which it is evident that no single model is capable of capturing the complexity of the observed behaviour. Some models are better at representing single features, but a general of interpretation of behaviour is not apparent.

This variety of model performances calls for *ad hoc* studies of the different physical causes that may be at its origin. Such studies go beyond the scope of the present work, but a few words can be spent about some possible candidates for further investigations, as resulting from literature. First of all, the parametrization of sinks and sources of momentum resulting from surface drag, orography and gravity wave propagation may be considered. That the interaction with orography can influence blocking was found by Mullen (1994), who obtained an enhancement of blocking frequency by the use of "envelope" orography. An influence of tropical heat flux (in turn linked to SST's, precipitation etc.) on blocking can also be envisaged, as seen in the already quoted work by Ferranti et al. (1992) who analysed mainly the Western Tropical Pacific. A possible mechanism for explaining such interactions may be linked to the influence of PNA on extended range predictability (see Palmer 1989; Palmer and Tibaldi 1988). Finally tropical variability has been addressed in the context of AMIP by Slingo et al. (1995) for the intraseasonal time scale. Nine of the models participating in this study are also analysed in Slingo et al.'s (1995) study and as

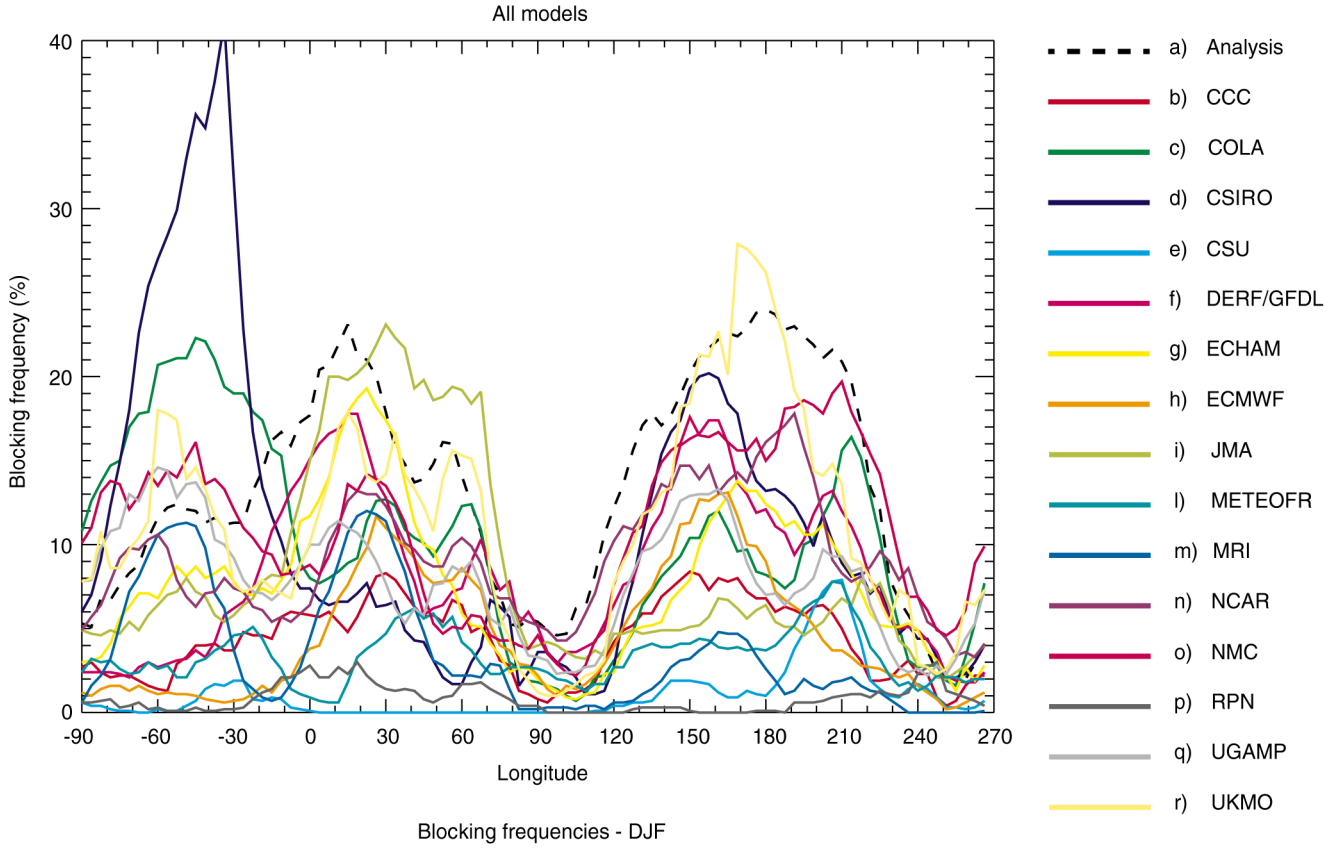

Fig. 11 Comparison diagram of longitudinal blocking frequency. Same as Fig. 5 but collapsed into one panel

a general rule the models with a low tropical variability also have a poor blocking simulation, with the possible exception of RPN. Of course this remark does not in itself suggest any physical cause-effect relationship between blocking and tropical variability.

Going back to blocking, and to the variety of model behaviours, it is possible to recognise some common model deficiencies. Firstly, all models tend to underestimate blocking frequency. This appears in practically all indicators, notably in the longitude diagrams of Figs. 4 and 11. Exceptions to this are present in some cases, mostly confined to the West Atlantic (Greenland) region. This underestimation is unaffected by the elimination of short (less than five days) blocks from the statistics. A dependency of this problem on model horizontal resolution is not evident. However, limiting the attention to grid-point models only (UKMO, MRI, CSU), the UKMO model performs better than the other two models of lower resolution. The case of spectral models is less clear and higher resolution models do not appear to perform systematically any better (see for example RPN and JMA).

The overestimation of blocking frequency in the WA sector is found to be an effect of an excessive amplitude of the Greenland ridge at the eastern edge of the North American continent in certain models. This problem has a clear counterpart in the mean (systematic) error maps of the models and their low-frequency variability. A northward displacement of the jet so as to make it interact spuriously with Greenland orography, as well as difficulties in the representation of orographic forcing itself, could both be possible reasons for this error.

When attention is focused on main sector blocking (Euro-Atlantic and Pacific) episodes, it becomes evident that most models have problems in producing long-lived blocking episodes with the observed frequency, with the exceptions of UKMO, NCAR and possibly DERF/GFDL. Despite the underestimation of duration, most models produce an exponentially decaying distribution of blocking lifetimes, in accord with observations. For many models, however, this diagnosis is made difficult by the overall paucity of blocking events. While many models tend to shift Euro-Atlantic blocking to the east of the observed position, no such general tendency is found for Pacific blocking. In this case, positive and negative errors in modelled blocking amplitude (intensity) are equally likely.

Appendix

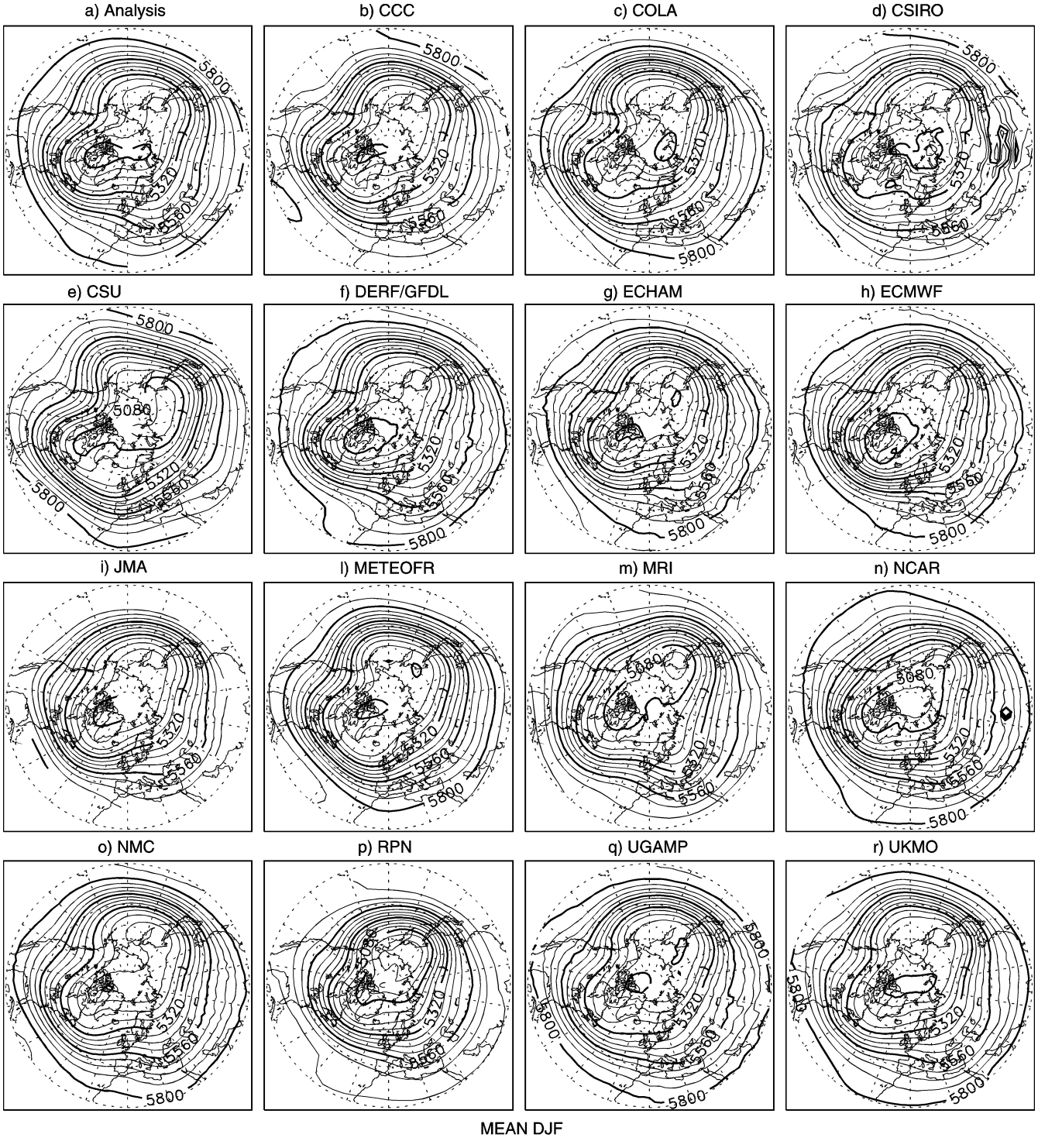

Fig. A1a–r Mean 500 hPa geopotential height of the DJF period for the analysis and the various models. Contour every 60 m

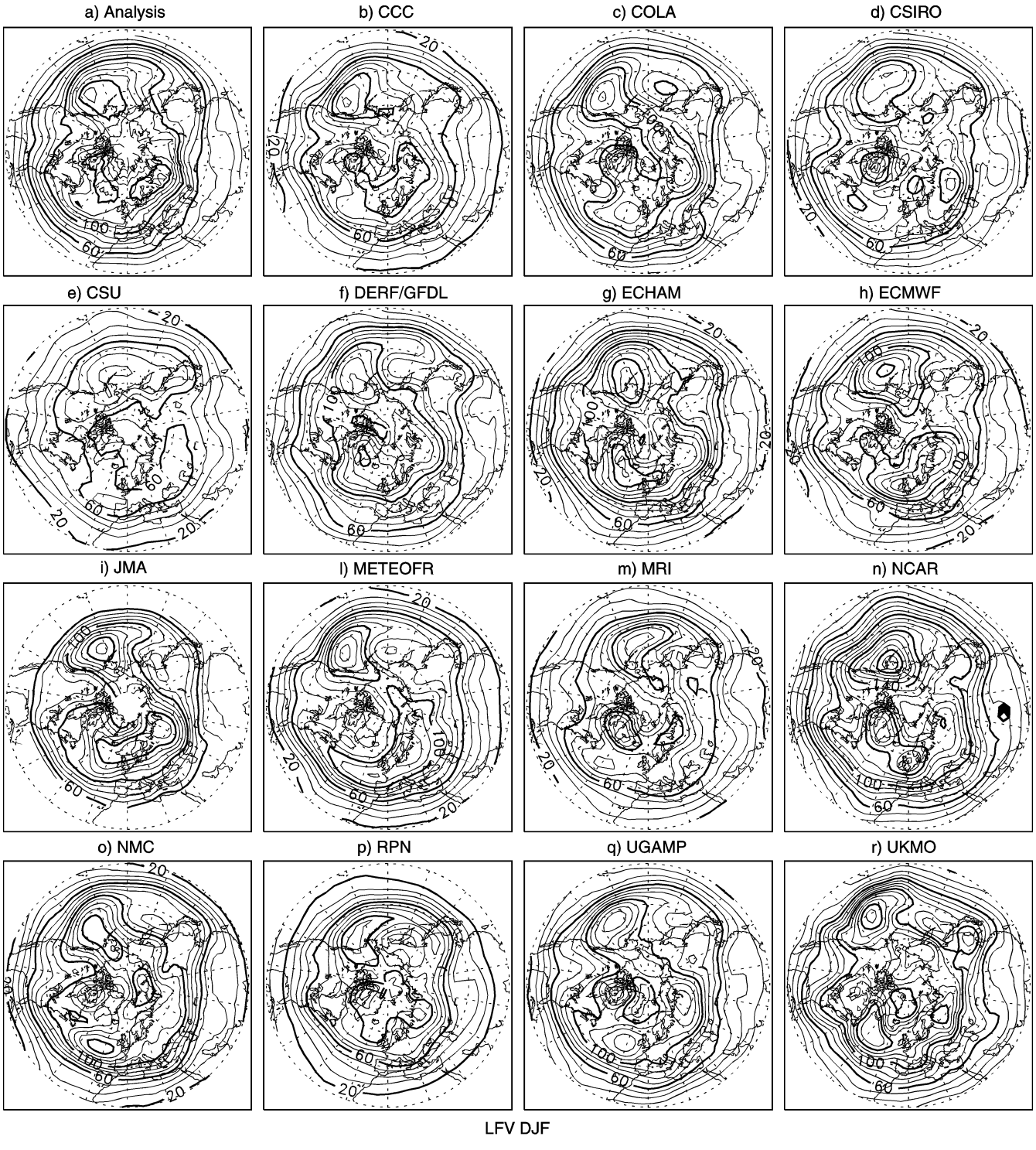

Fig. A2a–r Low frequency standard deviation (periods longer than 5 days) for analysis and participating models. Contour every 10 m

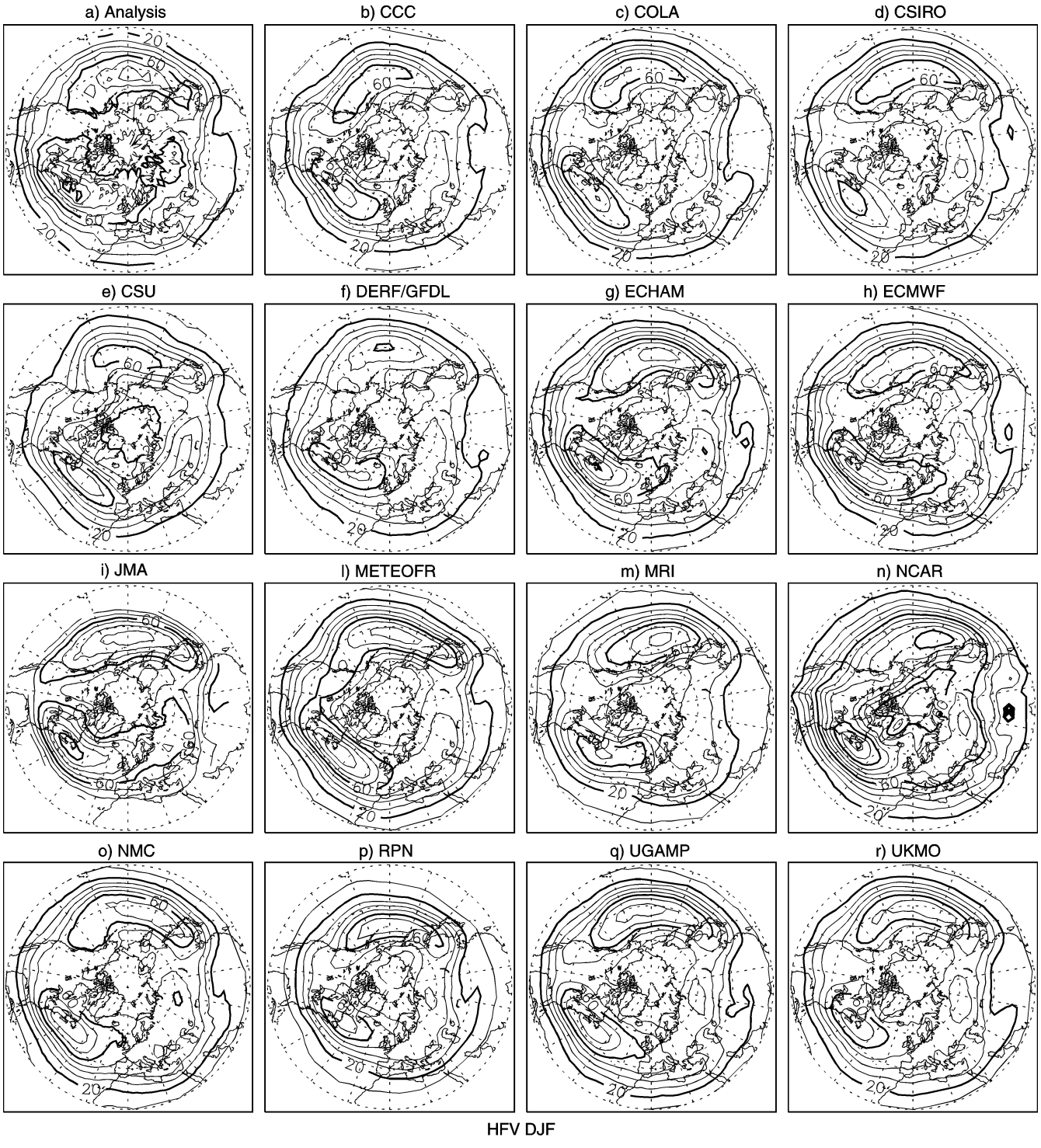

Fig. A3a–r High frequency standard deviation (periods shorter than 5 days) for analysis and participating models. Contour every 10 m

Acknowledgements The authors wish to thank Larry Gates and all the staff of PCMDI for contributing to the visits by FDA and ST to the Lawrence Livermore National Laboratory and Ken Sperber and Maggie Yatabe for their help in managing the history datsets. Acknowledgments also go to Prof. Kikuro Miyakoda and François Lott for useful advice and discussion. Special thanks to David Stephenson for the precious ideas and discussions, and for a thorough revision of the manuscript. Other people who contributed in various ways to the work are Marco Lazzeri, Masato Sugi, Mary Ann Huntley, Steve Lambert, and Jae Schemm. This work has been supported by EC Environment Contract EV5V-CT93-0279.

References

Anderson JL (1993) The climatology of blocking in a numerical forecast model. J Clim 6 : 1041–1056

Blackmon ML, Mullen ST and Bates GT (1986) The Cimatology of blocking in a perpetual January simulation of a spectral general circulation model. J Atmos Sci 43 : 1379–1405

Boyle JS (1995a) Intercomparison of the spectral characteristics of 200 Pa kinetic energy in AMIP GCM simulations, PCMDI Rep 23

Boyle JS (1995b) Estimated of zonally averaged tropical diabatic heating in AMIP GCM simulations, PCMDI Rep 25

Brankovic C, Ferranti L (1991) Seasonal integrations with realistic boundary forcing. ECMWF Workshop on New developments in predictability, pp 305–333

D'Andrea F, Tibaldi S, Blackburn M, Boer G, Dequé M, Dix MR, Dugas B, Ferranti L, Iwasaki T, Kitoh A, Pope V, Randall D, Roeckner E, Straus D, Stern W, van den Dool H, Williamson D (1996) Northern Hemisphere atmospheric blocking as simulated by 15 atmospheric general circulation models in the period 1979–1988. WCRP-96. WMO/784 WMO, Geneva

Déqué M, Piedelièvre JP (1995) High resolution climate simulation over Europe. Clim Dyn 11 : 321–339

Déqué M, Dreveton C, Braun A, Cariolle D (1994) The ARPEGE/IFS atmosphere model: a contribution to the French community climate modelling. Clim Dyn 10 : 246–266

Dole RM, Gordon ND (1983) Persistent anomalies of the extratropical Northern Hemisphere wintertime circulation: geographical distribution and regional persistence characteristics. Mon Weather Rev 111 : 1567–1586

Ferranti L, Molteni F, Palmer TN (1994) Impact of localised tropical SST anomalies in ensembles of seasonal GCM integrations. QJR Meteorol Soc 120 : 1613–1645

Gates WL, (1991) The validation of atmospheric models. Proc 1st Demetra meeting on the dilemma of Global Warming. Chianciano Terme, Italy, 28 October - 1 November 1991

Gates WL (1992) AMIP: the Atmospheric Model Intercomparison Project. Bull Am Meteorol Soc 73 : 1962–1970

Giannini A (1994) Variabilità a bassa frequenza nell'atmosfera invernale delle medie latitudini e sua modellistica. Tesi di Laurea, Available from the Department of Physics, University of Milan, Italy (in Italian)

Green JSA (1977) The weather during July 1976: some dynamical considerations of the drought. Weather 32 : 120–128

Hoskins BJ, James IN, White GH (1983) The shape, propagation and mean-flow interaction of large scale weather systems. J Atmos Sci 40 : 1595–1612

JMA (1993) Outline of operational weather prediction at Japan Meteorological Agency. Appendix to Progress Report on Numerical Weather Prediction, 128 pages

Kalnay E, Kanamitsu M, Kistler R, Colins W, Deaven D, GandinL, Iredell M, Saha S, White G, Woollen J, Zhu Y, Chelliqh M, Ebisuzaki W, Higgins W, Janowiak J, Mo KC, Ropelewski C, Wang J, Leetmaa A, Reynolds R, Jenne R, Joseph D (1996) The NCEP/NCAR 40-years reanalysis project. Bull Am Meteorl Soc 77 : 437–471

Mak M (1990) Dynamics of an atmospheric blocking as deduced from its local energetics. QJR Meteorol Soc 117 : 477–493

May W (1994) On the intraseasonal variability within the extratropics in the ECHAM3 general circulation model. Max-Planck-Institut für Meteorologie, Rep 147

Miyakoda K, Sirutis J (1990) Subgrid scale Physics in the month forecast. Part II: Systematic error and blocking forecast. Mon Weather Rev 118 : 1065–1081

Mullen SL (1986) The local balance of vorticity and heat for blocking anticyclones in a spectral general circulation model. J Atmos Sci 43 : 1406–1441

Mullen SL (1994) The impact of an envelope orography on low-frequency variability and blocking in a low-resolution general circulation model. J Atmos Sci 7 : 1815–1825

Palmer TN (1989) Medium and extended range predictability and stability of the Pacific/North American mode. QJR Meteorol Soc 114 : 691–713

Palmer TN Tibaldi S (1988) On the prediction of forecast skill. Mon Weather Rev 116 : 2453–2480

Phillips TJ (1994) A summary documentation of the AMIP models. PCMDI report no. 8, PCMDI Lawrence Livermore National Laboratory, USA

Rex DR (1950a) Blocking action in the middle troposphere and its effect upon regional climate. I. An aerological study of blocking action. Tellus 2 : 169–211

Rex DR (1950b) Blocking action in the middle troposphere and its effect upon regional climate. II. The climatology of blocking action. Tellus 2 : 275–301

Sausen R, König W, Sielmann F (1993) Analysis of blocking events from observations and ECHAM model simulations, Max-Planck-Institut für Meteorologie, Rep. 11, Hamburg (also in print in Tellus)

Shutts GJ (1986) A case study of eddy forcing during an atlantic blocking episode. Adv Geophys 29 : 135–161

Slingo J, Sperber KR, Boyle JS, Ceron J-P, Dix M, Dugas B, Ebisuzaki W, Fyfe J, Gregory D, Gueremy J-F, Hack J, Harzallah A, Inness P, Kitoh A, Lau WK, McAvaney B, Madden R, Matthews A, Palmer TN, Park C-K, Randall D, Renno N (1995) Intraseasonal oscillations in 15 atmospheric general circulation models (results from an AMIP diagnostic subproject). WMO-WCRP Rep 88

Sperber KR, Palmer TN (1995) Interannual tropical rainfall variability in general circulation model simulations associated with the Atmospheric Model Intercomparison Project. PCMDI Rep 28

Tibaldi S, Molteni F (1990) On the operational predictability of blocking. Tellus 42A : 343–365

Tibaldi S, Tosi E, Navarra A, Pedulli L (1994) Northern and southern hemisphere seasonal variability of blocking frequency and predictability. Mon Weather Rev 122 : 1971–2003

Tibaldi S, Ruti P, Tosi E, Maruca MM (1995) Operational predictability of winter blocking. Ann Geophys 13 : 305–317

Tibaldi S, D'Andrea F, Tosi E, Roeckner E (1997) Climatology of Northern Hemisphere blocking in the ECHAM model. Clim Dyn (1997) 13 : 649–666

Tracton MS (1990) Predictability and its relationship to scale interaction processes in blocking. Mon Weather Rev 118 : 1666–1695

Tracton MS, Mo K, Chen W, Kalnay E, Klister R, White G (1989) Dynamical extended range forecasting (DERF) at the National Meteorological Center Mon Weather Rev 117 : 1604–1635

Vautard R (1990) Multiple weather regimes over the North Atlantic. Analysis of precursors and successors. Mon Weather Rev 118 : 2056–2077

Wallace JM, Gutzler DS (1981) Teleconnections in the geopotential height field during the northern hemisphere winter. Mon Weather Rev 109 : 784–812